Journal of Applied Polymer Science

Synergetic effects on the mechanical and fracture properties of epoxy composites with multiscale reinforcements: Carbon nanotubes and short carbon fibers

Zhongwei Zhang, Yefa Tan, Xiaolong Wang, Yanyan Lin, Lulu Wang
College of Field Engineering, PLA University of Science and Technology, Nanjing 210007, China
Correspondence to: Y. Tan (E-mail: tanyefa7651@163.com)

ABSTRACT: The ball-milling/liquid-phase oxidation (BMLPO) method was used to fabricate surface-modified short carbon fibers (SCFs). Multiscale epoxy composites reinforced with a combination of SCFs and multiwalled carbon nanotubes (MWNTs) were prepared. Atomic force microscopy observations and contact angle measurement were used to investigate the modification effect of the BMLPO method. Mechanical tests and scanning electron microscopy observations were used to study the effects of the SCFs, MWNTs, and their combination on tensile properties, impact strength, and fracture toughness of the epoxy composites. The results show that the surface roughness of the SCFs after BMLPO treatment increased, and the wettability of the SCFs was improved as well. The combined use of the SCFs and MWNTs had a synergetic effect on the tensile strength, fracture toughness, and impact strength of the epoxy composites. The addition of MWNTs promoted the plastic deformation of the epoxy matrix and decreased the stress-concentration level near the SCF/matrix interface; these were considered the main causes of the synergetic effect. © 2016 Wiley Periodicals, Inc. J. Appl. Polym. Sci. **2016**, *133*, 43500.

KEYWORDS: fibers; graphene and fullerenes; mechanical properties; nanotubes; resins

Received 14 October 2015; accepted 31 January 2016
DOI: 10.1002/app.43500

INTRODUCTION

Epoxy resins (EPs) show a wide range of advantages, including a low weight, high bonding strength, and good chemical resistance; thus, they have been widely used as adhesives, coatings, and electronic encapsulation materials.[1–3] However, EPs also display undesirable properties, including brittle fracture behavior and poor crack-propagation resistance; this hampers their potential in high-performance applications.[4,5] Therefore, necessary modification methods are usually used to improve their mechanical and fracture performance; these methods include fiber reinforcing and nanofiller modification.

In comparison with continuous carbon fiber-reinforced composites, short carbon fiber (SCF)-reinforced composites show superiority in their low cost, approximate isotropy, and uncomplicated preparation techniques. Therefore, they have attracted increasing attention in the automobile, furniture, and construction industries.[6–8] Micrometer-sized SCFs can increase the modulus and impact strength of the EPs simultaneously.[9] Compared with spherical micrometer-sized particles, the reinforcing mechanisms of SCFs are more complex. Researchers have found that fiber pull-out, fiber debonding, and fiber breakage play key roles in the reinforcement of polymer composites.[10,11] However, because of the large differences in the elastic modulus and thermal expansion coefficient values between the SCFs and the matrix, serious stress concentrations usually exist near the SCF/matrix interfaces; this damages the mechanical performance of the composites.

Recently, carbon nanotubes (CNTs) are usually used as reinforcements to modify EPs. CNTs are a category of quasi-one-dimensional filament materials with excellent mechanical, thermal, and electronic properties.[12] As one of the stiffest and strongest fibers, they have attracted much attention in science and engineering.[13–15] Compared with spherical nanoparticles, such as nano-SiO_2 or nano-Al_2O_3, CNTs have a large length-to-diameter ratio and specific surface area; these contribute to the enhancement of the stress transmission ability of the CNT/matrix interfaces.[16–18] Many studies have shown that the strength and toughness of the EPs were both improved by the addition of well-dispersed CNTs.[19–21] Despite the fact that much work has been done on CNT-reinforced EPs, the fracture toughness can only be enhanced by an insufficient degree; thus, more effective toughening methods are still required to further improve the fracture toughness of the EPs.

The attainment of both strength and toughness in EPs is a vital requirement in many application areas. However, these two

Table I. Compositions of the Studied Materials

Series	Material code	Matrix (phr)	Untreated SCFs (phr)	Treated SCFs (phr)	MWNTs (phr)
Neat epoxy	EP	100	—	—	—
Untreated SCF/EP composites	10CF	100	10	—	—
Treated SCF/EP composites	10TCF	100	—	10	—
MWNT/EP composites	0.5NT	100	—	—	0.5
	1NT	100	—	—	1
	1.5NT	100	—	—	1.5
Treated SCF/MWNT/EP composites	10TCF0.5NT	100	—	10	0.5
	10TCF1NT	100	—	10	1
	10TCF1.5NT	100	—	10	1.5

properties are generally mutually exclusive.[22] Therefore, it shows practical significance for simultaneously improving the strength and toughness of EPs without the sacrifice of other key properties. A promising method is the preparation of multiscale epoxy composites reinforced with both microsized and nanosized reinforcements. Recent studies have indicated that multiscale reinforcements contribute to improving the overall properties of the EPs. Rahmanian *et al.*[23] found that multiscale composites reinforced with both CNTs and CNT-grown SCFs revealed significant improvements in the elastic modulus, storage modulus, tensile strength, and impact resistance compared with the CNT–epoxy or CNT-grown SCF–epoxy composites. Zhang and coworkers[11,24] reported that multiscale carbon reinforcements led to remarkable synergetic effects on the tensile and fracture performances of EP. Several other researches showed that multiscale reinforcements contributed to improvements in the compressive strength,[25] shear strength,[26] or fracture toughness[27] of the epoxy composites. Although multiscale reinforcements have been reported to reinforce EPs effectively, their toughening and reinforcing mechanisms (especially their synergetic roles) are still unclear. Herein, further work is still required to obtain a deeper understanding of the reinforcing mechanisms in multiscale epoxy systems.

In this study, SCFs were surface-treated via physical and chemical methods. Multiwalled carbon nanotubes (MWNTs), untreated SCFs, and treated SCFs were used to prepare epoxy composites. The effects of multiscale reinforcements on the tensile properties, dynamic mechanical performance, fracture toughness, and impact strength were investigated. The main aim of this study was to further explore the reinforcing and toughening mechanisms of multiscale fillers to reveal their synergetic roles in the overall improvement of the mechanical and fracture properties.

EXPERIMENTAL

Materials

The SCFs (T700SC-12000-50C, short segments 3 mm in length) were produced by Toray Co., Ltd. (Japan). Their tensile strength and elastic modulus values were 5.07 and 232 GPa, respectively. The EP used in this study was a bisphenol A EP (WSR618) with an epoxy equivalent of 185–192 g/equiv; it was purchased from Bluestar Wuxi Petrochemical Co., Ltd. (China). The curing agent was FS-2B from Chuzhou Hui-Sheng Electronic Materials Co., Ltd. (China); it was a modified cycloaliphatic amine curing agent with a mixing ratio by weight to WSR618 of 1:1. The carboxylic-functionalized MWNTs were provided by XFNANO Materials Tech Co., Ltd. (China); it had an average diameter of 10–20 nm and a length of 0.5–2 μm.

Surface Treatment of the SCFs

First, the SCFs were surface-desized in a Soxhlet extractor for 72 h with acetone as the extraction medium. Then, they were milled by a planetary ball mill (QM-ISP4, Nanjing University Instrument Plant, China) for 10 min in an aluminum milling pot after drying. The SCFs obtained were divided into two groups. One part was directly used to fabricate SCF-reinforced epoxy composites, and the other part was immersed in nitric acid (40 vol %) for 25 min with a coupling agent (KH550, 25 vol %) for 1 h, respectively. After this procedure, the surface-treated SCFs were washed with deionized water and dried in an oven at the temperature of 100 °C.

Specimen Preparation

The specimens in this study were prepared according to Table I. First, the blend was stirred by a high-speed motor stirrer for 24 h at a speed of 2000 rpm; it was then processed by ultrasonic treatment for 2 h at 60 °C. Then, the blend was mixed with the curing agent. Finally, the samples were cured in a stainless steel mould for 1 h at 60 °C and 2 h at 150 °C.

Characterization

The tensile properties were tested on a SANS CMT5105 universal testing machine at a temperature of 23 °C according to ASTM D 638-2010 standard. The measurements were performed at a speed of 5 mm/min, and at least five specimens were tested for each composition. Dynamic mechanical analysis (DMA) was performed on a TA-Q800 dynamic mechanical analyzer with single-cantilever bending mode, and the amplitude was 5 μm. The dimensions of the specimens were $33 \times 10 \times 2\ mm^3$. The experiment were conducted with various temperatures from 10 to 200 °C at a rate of 3 °C/min. The fracture toughness was determined by way of the single-edge-notched bend specimens in accordance with ASTM D 5045-99. The rectangular samples were cured in a steel mold with dimensions of $60 \times 10 \times 5\ mm^3$. The tests were performed at a rate of 10 mm/min. At least five measurements were tested for each

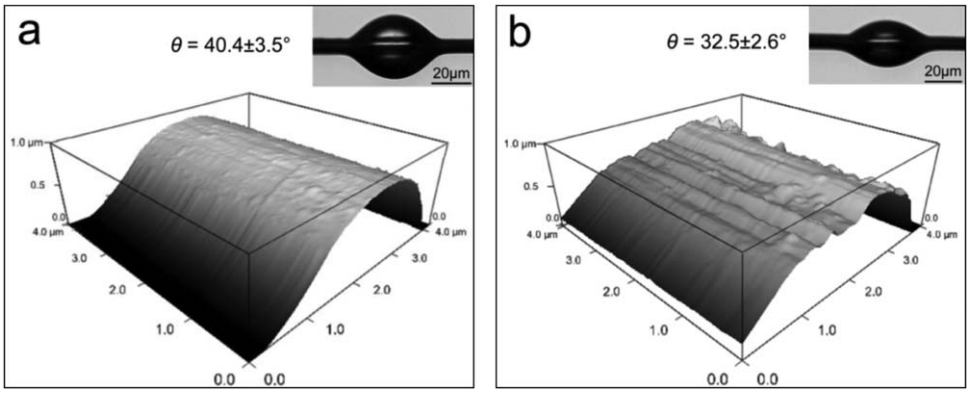

Figure 1. AFM photographs of the SCF surfaces and the corresponding contact angles (θ) of epoxy against the SCFs: (a) pristine and (b) treated fibers.

composition. The fracture toughness was calculated in terms of plane-strain fracture toughness (K_{IC}), and this equation follows, where, Y represents the shape factor of the cracks, S is the support span of the three-point bending, t is the specimen thickness, w is the specimen width, and a represents the crack length.[28] Poisson's ratio was 0.35[29]:

$$K_{IC} = Y\frac{6P_f S}{4tw^2}\sqrt{a} \quad (1)$$

The impact strengths of the materials were measured by an XJ-6608C impact instrument, and both the notched and unnotched samples were tested at a temperature of 25 °C. The geometries of the impact samples were $80 \times 10 \times 4\ mm^3$ according to ASTM D 256. Particularly in this research, the tensile, fracture, and impact specimens were tested before and after relaxation in an oven at 60 °C for 30 min to relieve their internal stress.

The microstructures of the SCF surfaces were examined with atomic force microscopy (AFM; MFP-3D-SA). The fracture surfaces of the specimens were investigated with scanning electron microscopy (SEM; Hitachi S4800, Japan), and a thin layer of gold was coated on the samples before the observations to prevent charging.

RESULTS AND DISCUSSION

Surface Treatment of the SCFs

Figure 1 shows the morphology of the SCF surfaces and the corresponding contact angles of epoxy against the SCFs before and after ball-milling/liquid-phase oxidation (BMLPO) treatment. The untreated pristine fiber presented a cylinder-shaped appearance with a smooth surface [Figure 1(a)], and the corresponding surface roughness values and contact angle were 73 nm (Table II) and 40.4°, respectively. After surface treatment by the BMLPO method, the surface roughness of the SCFs increased to 418 nm (Table II), with many particles remaining on it, and some grooves were observed along the radial direction. Meanwhile, the contact angle decreased to 32.5° [Figure 1(b)]. This phenomenon was attributed to the combination of the milling behavior and the oxidation effect on the amorphous carbon of the SCF surfaces. Generally, an SCF is composed of a proper fiber in the center and the amorphous carbon deposited on it.[30] Figure 2 illustrates the cross-sectional diagram of an SCF before and after BMLPO treatment. Compared with those of the pristine fibers, the increased surface roughness and improved wettability of the treated SCFs contributed to improving the stress transmission ability of the SCF/matrix interface.

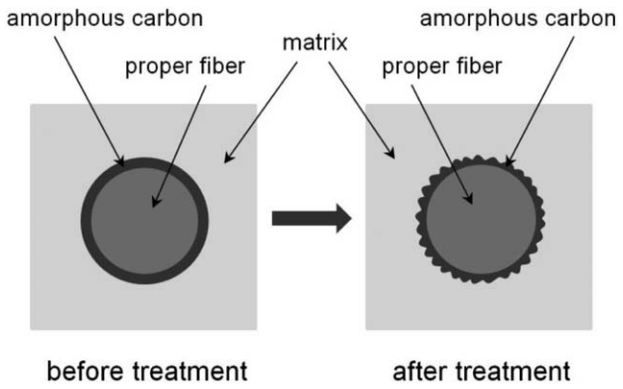

Figure 2. Diagram of the mechanism of the milling/liquid-phase oxidation treatment on the carbon fibers.

Tensile Properties

Figure 3 displays the stress–strain curves, tensile strength (before and after relaxation), elastic modulus, and elongation at break of the materials studied. It shows that the specimen of EP presented a typical brittle fracture characteristic [Figure 3(a)]. With regard to the specimens reinforced with CNTs (1NT), untreated SCFs (10CF), and treated SCFs (10TCF), there were no essential changes in the shapes of the stress–strain curves. However, the multiscale reinforced specimen (10TCF1NT) showed a different fracture model. The yielding characteristic of the stress–strain curve indicated the transformation of fracture model from brittle to ductile behavior.

As shown in Figure 3(b), all of the reinforced specimens were enhanced in tensile strength compared to the neat EP. The tensile strength of the treated SCF-reinforced specimen (10TCF) showed a better reinforcing effect than the untreated SCFs; this was attributed to the improved wettability and enlarged surface

Table II. Root Mean Square Roughness of the SCF Surfaces

SCF type	Pristine fiber	Treated fiber
Root mean square roughness (nm)	73	418

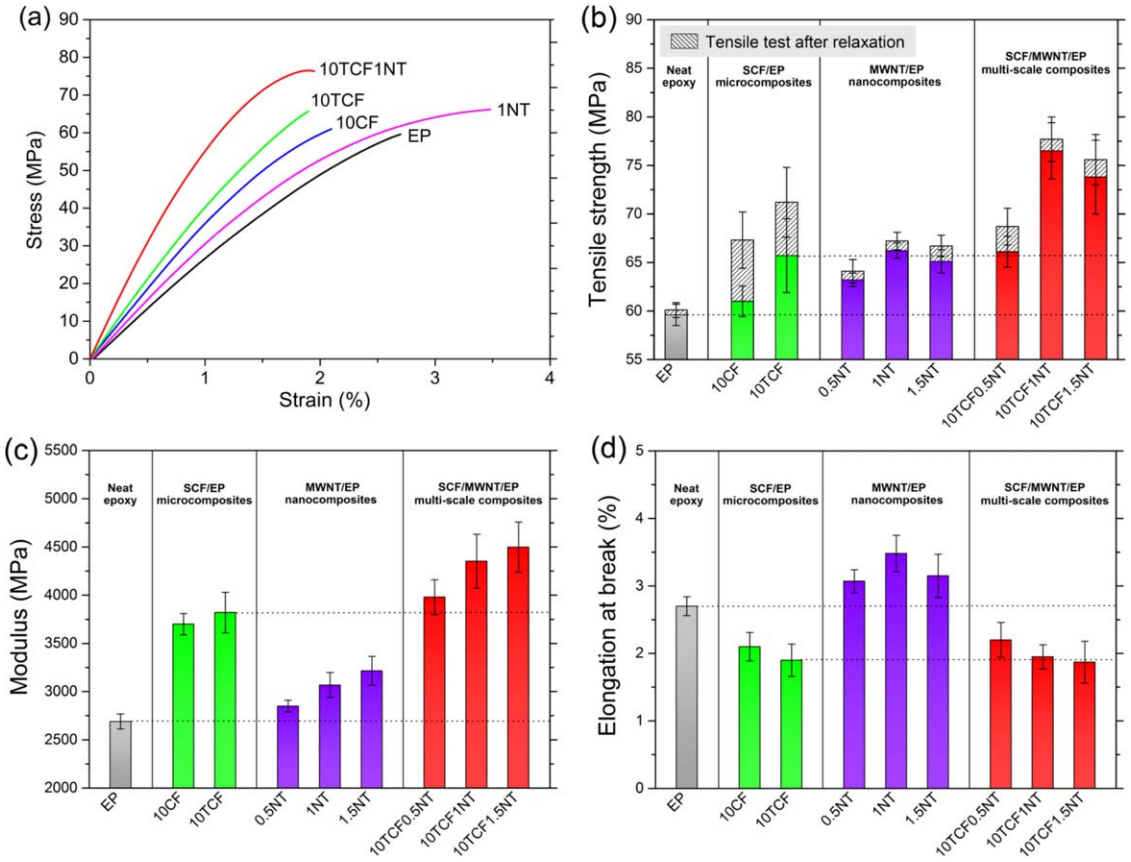

Figure 3. Tensile properties of the studied materials: (a) stress–strain curves of some typical materials, (b) tensile strength before and after relaxation, (c) elastic modulus, and (d) elongation at break. [Color figure can be viewed in the online issue, which is available at wileyonlinelibrary.com.]

roughness of the treated SCFs. The addition of MWNTs slightly increased the tensile strength of the neat EP. As the MWNT content increased from 0.5 to 1.5 phr, the tensile strength first increased and then decreased; it achieved a maximum value at an MWNT content of 1 phr. Compared with the solely reinforced specimens, the multiscale reinforced specimens presented more outstanding reinforcing effects on the tensile strength. For example, the tensile strength of 10TCF1NT reached 76.5 MPa; this was a 28.4% increase compared to that of the neat EP. It is noteworthy that this increment was higher than the sum of the tensile strength growth of both 10TCF (with the sole addition of 10-phr treated SCFs, there was an increase of 10.2% over that of EP) and 1NT (with the sole addition of 1-phr MWNTs, there was an increase of 11.1% over that of EP). This result indicates that the combination of the treated SCFs and MWNTs played a synergetic role in the tensile strength of the EP.

Because of the huge difference in the thermal expansion coefficient and modulus between the filled reinforcements and the matrix, internal stress occurred in the cured composites with volume shrinkage and temperature variation in the curing process. In particular, for the SCF-reinforced epoxy composites, an internal stress usually forms at the SCF/EP interfaces; this generates serious stress concentration, which damages the mechanical performance of the materials.[31] As shown in Figure 3(b), the tensile strengths of all of the specimens increased after relaxation. Generally, the difference in the tensile strength between stress-relaxed specimens and specimens without relaxation reflects the internal stress level of the materials. We found that the SCF-reinforced specimens displayed a higher internal stress level than any of the other samples; this implied that critical failures occurred more easily in their high stress-concentration areas, for example, the SCF/EP interfaces. Compared with the high internal stress level of the SCF-reinforced specimens, the multiscale reinforced specimens showed an obvious decrease. On the one hand, this phenomenon was attributed to the internal stress redistribution triggered by the strong stress-transfer ability of the MWNTs during the curing process;[32] this helped to relieve the overstress at the SCF/EP interfaces. On the other hand, the internal stress in the cured composites could be divided into two parts, that is, the volume-shrinkage-caused internal stress and the difference in the coefficient of thermal expansion caused by internal stress.[31] The addition of MWNTs decreased the volume shrinkage,[32] and the coefficient of thermal expansion[33] of the epoxy matrix contributed to a reduction in the internal stress level of the cured composites according to Jyotishkumar *et al.*[34]

Figure 3(c,d) illustrates the elastic modulus and elongation at break of the materials in Table I, respectively. It shows that the elastic modulus values of all of the reinforced specimens were enhanced. However, only the MWNT-reinforced specimens were improved in the elongation at break. The elastic modulus of a short fiber-reinforced binary composite can be predicted by the

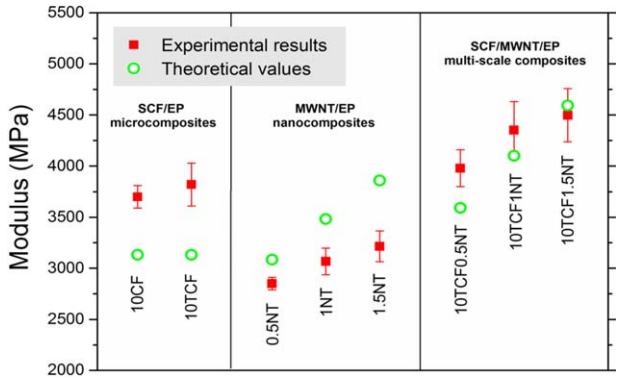

Figure 4. Theoretical values and experimental results for the elastic modulus. [Color figure can be viewed in the online issue, which is available at wileyonlinelibrary.com.]

Halpin–Tsai equations,[35] but it is not applicable for a ternary system reinforced with two kinds of fibers. In this study, a modified model was developed on the basis of the Halpin–Tsai equations to broad their applications to ternary systems. As an assumption, for the EP filled with randomly oriented MWNTs, the MWNT/epoxy interfaces were perfectly bonded (a detailed discussion on the interfacial interactions is shown in the DMA section), and the tension loading resulted in the generation of interfacial shear stresses in the materials.[36] Then, the following equations were obtained:

$$\frac{E_c}{E_{m_1}}=\frac{3}{8}\left[\frac{1+2(l_1/d_1)\eta_{L_1}\phi_{SCF}}{1-\eta_{L_1}\phi_{SCF}}\right]+\frac{5}{8}\left(\frac{1+2\eta_{T_1}\phi_{SCF}}{1-\eta_{T_1}\phi_{SCF}}\right) \quad (2)$$

$$\eta_{L_1}=\frac{E_{SCF}/E_{m_1}-1}{E_{SCF}/E_{m_1}+2(l_1/d_1)} \quad (3)$$

$$\eta_{T_1}=\frac{E_{SCF}/E_{m_1}-1}{E_{SCF}/E_{m_1}+2} \quad (4)$$

For the ternary composite reinforced with the combination of SCFs and MWNTs, with the assumption that the composite reinforced with MWNTs could be treated as a new matrix (m_1), and then, the treated SCFs were considered the sole reinforcement for the new matrix-based system. Thus, the ternary problem was transformed into a binary one. E_{m1}, E_c, and E_{SCF} were the elastic moduli of the new matrix, the ternary composite, and the SCFs (GPa), respectively. l_1 and d_1 represents the average length and diameter of the treated SCFs, respectively. ϕ_{SCF} is the volume fraction of the introduced SCFs. For the epoxy system solely reinforced with MWNTs, the following equations were obtained:

$$\frac{E_{m_1}}{E_{m_0}}=\frac{3}{8}\left[\frac{1+2(l_2/d_2)\eta_{L_2}\phi_{CNT}}{1-\eta_{L_2}\phi_{CNT}}\right]+\frac{5}{8}\left(\frac{1+2\eta_{T_2}\phi_{CNT}}{1-\eta_{T_2}\phi_{CNT}}\right) \quad (5)$$

$$\eta_{L_2}=\frac{E_{CNT}/E_{m0}-1}{E_{CNT}/E_{m0}+2(l_2/d_2)} \quad (6)$$

$$\eta_{T_2}=\frac{E_{CNT}/E_{m0}-1}{E_{CNT}/E_{m0}+2} \quad (7)$$

where E_{m0} and E_{CNT} are the elastic moduli of the neat EP and MWNTs (GPa), respectively; l_2 and d_2 are the average length and diameter, respectively, of the MWNTs; and ϕ_{CNT} is the volume fraction of the introduced MWNTs. In this study, the elastic moduli of the neat EP, MWNTs, and treated SCFs were 2.69 GPa (by the experimental results), 1 TPa,[37] and 232 GPa, respectively. The average length and diameter of the MWNTs were assumed to be 1.5 μm and 15 nm, respectively. The average length and diameter of the treated SCFs were 7 μm (as determined by AFM observations) and 950 μm (as determined through the calculation of the average length of 100 SCFs), respectively. Then, the relationship between the elastic modulus of the ternary composite and the neat EP was obtained, as indicated in eq. (8):

$$E_c=E_{m_0}\left[\frac{3}{8}\times\frac{1+2(l_1/d_1)\eta_{L_1}\phi_{SCF}}{1-\eta_{L_1}\phi_{SCF}}+\frac{5}{8}\times\frac{1+2\eta_{T_1}\phi_{SCF}}{1-\eta_{T_1}\phi_{SCF}}\right]\left[\frac{3}{8}\times\frac{1+2(l_2/d_2)\eta_2\phi_{CNT}}{1-\eta_{L_2}\phi_{CNT}}+\frac{5}{8}\times\frac{1+2\eta_{T_2}\phi_{CNT}}{1-\eta_{T_2}\phi_{CNT}}\right] \quad (8)$$

Figure 4 shows the comparative results between the experimental and theoretical values. For the specimens solely reinforced with SCFs or MWNTs, most of the relative errors between the experimental and theoretical values were larger than 10%, as shown in Table III. These major errors could have indicated that the precondition of the Halpin–Tsai equations were not well satisfied, so the interface failure could have occurred at the filler/matrix interfaces because they were imperfectly bonded. For the multiscale epoxy composites reinforced with both treated SCFs and MWNTs, the relative errors between the experimental and theoretical values were all smaller than 10%. In particular, with regard to the specimens of 10TCF1NT and 10TCF1.5NT, the relative errors were only 5.7 and −2.1%, respectively. These results suggest that the interactions between the mircosized SCFs and the nanosized MWNTs contributed to the minimization of the incidence rate of interface debonding, and thus, the well-satisfied precondition of the Halpin–Tsai equations led to these small relative errors.

DMA

Figure 5 illustrates the tan δ curves of the composites as a function of the temperature by means of DMA. The glass-transition temperature (T_g) was obtained from the peak of the tan δ curves. We found that the T_g values of EP increased with the addition of both the treated SCFs and the MWNTs, while they

Table III. Deviations of the Theoretical Values and Experimental Results for the Elastic Modulus

Material code	Experimental result (MPa)	Theoretical value (MPa)	Relative error (%)
10CF	3702	3130	15.5
10TCF	3818	3130	18.0
0.5NT	2851	3085	−8.2
1NT	3067	3481	−13.5
1.5NT	3215	3860	−20.1
10TCF0.5NT	3980	3591	9.8
10TCF1NT	4352	4102	5.7
10TCF1.5NT	4498	4592	−2.1

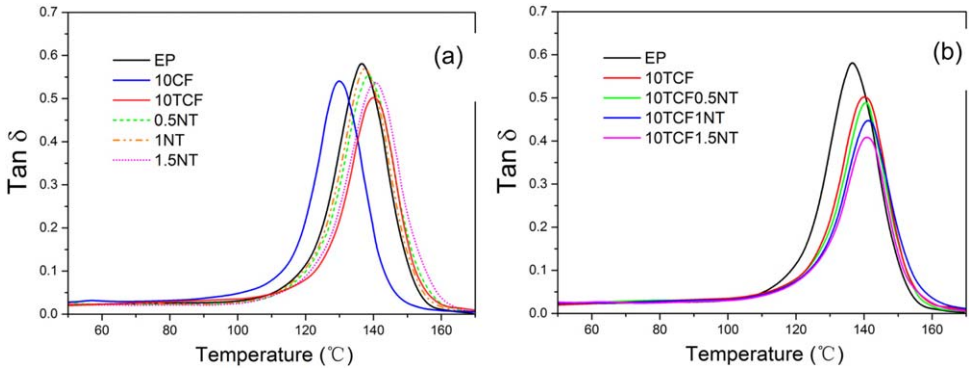

Figure 5. Tan δ curves of the composites as a function of the temperature: (a) solely reinforced specimens and neat EP and (b) influence of the content of the MWNT addition on the variation of the tan δ curves. [Color figure can be viewed in the online issue, which is available at wileyonlinelibrary.com.]

decreased with the addition of the untreated SCFs [Figure 5(a)]. In general, the T_g values indicated the start of large-scale motions of the molecular chains in the polymer materials.[38] For the treated SCF-reinforced specimen, the strong interactions of the SCFs and matrix tended to constrain the mobility of the polymer chains and, therefore, decreased T_g. With respect to the MWNT-reinforced specimens, the increase in T_g was believed to be the result of improved MWNT/EP interfacial interactions because the MWNTs used in this study were carboxylic-functionalized. The published literature revealed that the carboxylated MWNTs hindered the mobility of the reactive species at the MWNT/EP interface area and generated strong interfacial interactions in the epoxy composites.[39] Moreover, the decreased peak height of the tan δ curves (tan δ_{max}) for the MWNT-reinforced specimens was also considered evidence for the well-bonded interfaces according to Keusch and Haessler.[40]

The previous results indicate that for the specimens filled with the treated SCFs or MWNTs, strong interactions existed, and the layer of interphases was formed at the interfaces. According to Iisaka and Shibayama,[41] the effect of the interphase thickness on the damping (tan δ) was described as eq. (9):

$$\tan\delta_c = \tan\delta_m \left[1 - \left(1 + \frac{\Delta R}{R}\right)^2 V_f\right] \quad (9)$$

where tan δ_c and tan δ_m are the damping of the composites and the matrix, respectively; V_f is the volume fraction of the reinforcements; R is the radius of the SCFs or MWNTs; and ΔR represents the effective thickness of the interphase between the reinforcements and the matrix.

Equation (9) was used to calculate the interphase thickness in a binary composite; this was solely reinforced with MWNTs or fibers but did not apply to the multiscale composites filled with both SCFs and MWNTs. Inspired by the discussion of the modified Halpin–Tsai model as given previously, a similar method was also adopted to calculate ΔR in multiscale composites. With the assumption that the composite solely reinforced with MWNTs or treated SCFs could be treated as a new matrix, the other kind of fillers were considered as sole reinforcement for the new matrix-based system. By this means, the ternary problem was transformed into a binary one, and eq. (9) could be used.

The calculation values are listed in Table IV. This shows that ΔR of the treated SCFs (1628.4 nm) was much higher than that of the untreated SCFs (53 nm); this indicated a much stronger interfacial interaction. This was consistent with the damping and T_g results given previously. ΔRs of the MWNTs remained within the range 10–20 nm when the MWNT content was varied from 0.5 to 1.5 phr. It is worth noting that the ΔR values of the MWNTs were even larger than its average radius (7.5 nm); this implied a great reinforcing potential and efficient stress transferability. For the multiscale specimen of 10TCF0.5NT, the ΔR values of the SCFs and MWNTs were 1602.9 and 15.6 nm,

Table IV. Summary of the DMA Results for the Studied Materials

Specimen	T_g (°C)	Tan δ_{max}	V_f of the SCFs	V_f of the MWNTs	ΔR of the SCFs (nm)	ΔR of the MWNTs (nm)
EP	136.6	0.577	—	—	—	—
10CF	129.7	0.541	0.06054	—	53.0	—
10TCF	139.8	0.502	0.06054	—	1628.4	—
0.5NT	137.4	0.561	—	0.00269	—	16.6
1NT	139.1	0.550	—	0.00537	—	14.6
1.5NT	140.2	0.539	—	0.00803	—	13.9
10TCF0.5NT	140.6	0.489	0.06292	0.00273	1602.9	15.6
10TCF1NT	141.7	0.448	0.06528	0.00545	2642.5	25.8
10TCF1.5NT	141.2	0.423	0.06763	0.00815	3125.9	25.5

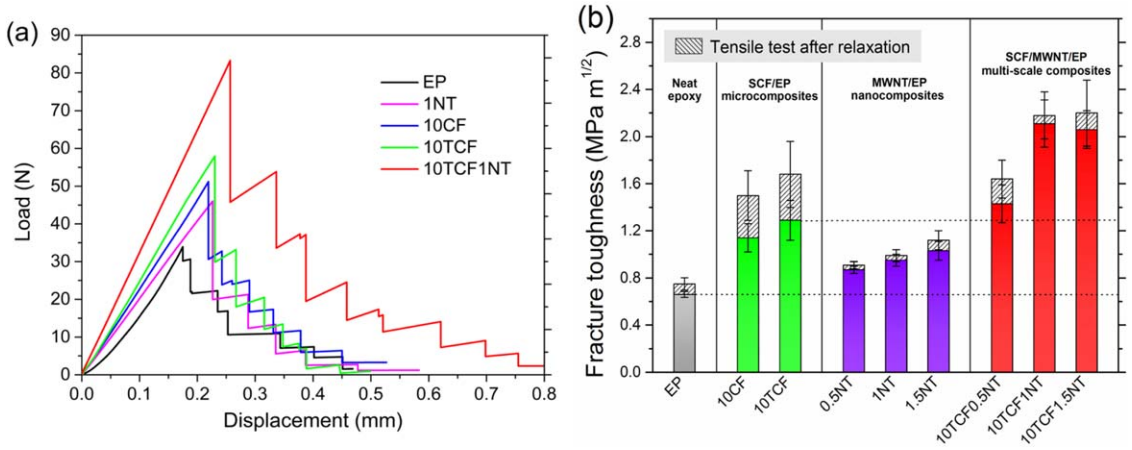

Figure 6. Fracture properties of the studied materials: (a) load–displacement curves of some typical materials and (b) fracture toughness. [Color figure can be viewed in the online issue, which is available at wileyonlinelibrary.com.]

respectively; these values were almost equal to corresponding results in the binary composites. However, for the multiscale specimens of 10TCF1NT and 10TCF1.5NT, the ΔR values of the SCFs and MWNTs showed significant increases compared with their corresponding results in the binary composites. For example, the ΔR values of the SCFs and MWNTs in the 10TCF1NT specimen were 2642.5 and 25.8 nm, respectively. However, in the binary specimens, the corresponding values were only 1628.4 and 16.6 nm, respectively. Therefore, the combined use of the treated SCFs and MWNTs promoted interfacial interactions with each other.

It is well known that the interfaces in a composite are transition layers between the reinforcements and the matrix. When the composite was applied with forces, the stress will transfer from the matrix to the reinforcements, mainly through the interphases. Because of the huge difference in the elastic modulus and the thermal expansion coefficient between the SCFs and the matrix, serious stress concentration usually existed at the SCF/EP interfaces. This always sharply decreased the fracture toughness of the composites. As the previous DMA results indicate, the effective thickness of the SCF/EP interphase significantly increased in the multiscale composites because of the addition of MWNTs; this implied that the stress was transferred through a larger transition zone. Therefore, the concentrated stress at the SCF/EP interfaces was redistributed, and the stress field was homogenized by the MWNTs.

Fracture Toughness

Figure 6(a) illustrates the typical load–displacement curves of the materials in Table I. This showed that the specimen of the neat EP displayed typical brittle fracture behavior. Comparatively, the fracture toughness values of the reinforced specimens all improved. The multiscale specimen of 10TCF1NT showed the best toughening effect. The fracture toughness values of the materials examined in this study are shown in Figure 6(b) in terms of K_{IC}. This showed that the K_{IC} of neat EP was 0.66 MPa $m^{1/2}$. Meanwhile, the K_{IC} of the composites reinforced with untreated and treated SCFs were 1.14 and 1.29 MPa $m^{1/2}$; these were increases of 72.7 and 95.5% over than that of the neat EP, respectively; this indicated that the treated SCFs were superior in toughening effect over the untreated ones. Generally, the toughening mechanisms of the SCFs included fiber pullout, fiber breakage, and fiber debonding. We found from the previous results (Figure 1 and Table II) that the treated SCFs showed a larger surface roughness and better wettability than the untreated ones; thus, the SCF/EP interfaces were better integrated. and this consumed more energy when the SCFs pulled out or debonded from the epoxy matrix. Therefore, in the macroscopic view, the treated SCF-reinforced EPs displayed a higher fracture toughness than the untreated SCF-reinforced ones.

The K_{IC} values of the MWNT-reinforced specimens (0.5NT, 1NT, and 1.5NT) were 0.87, 0.95, and 1.03 MPa $m^{1/2}$; these represented 31.8, 43.9, and 56.1% increases over that of the neat EP, respectively. The K_{IC} increment of 1NT was about one-half that of 10TCF, but the addition content of MWNTs was only one-tenth that of the untreated SCFs. This phenomenon implied that the MWNTs were more efficient in toughening the EPs than the microsized SCFs. Compared with the composites solely filled with SCFs or MWNTs, the multiscale specimens filled with a combination of treated SCFs and MWNTs showed a more significant improvement in fracture toughness. The K_{IC} of 10TCF1NT reached 2.11 MPa $m^{1/2}$, increasing by 219.7% over than that of the neat EP; this was higher than the total growth of 10TCF and 1NT (219.7% > 95.5% + 43.9%). Therefore, the treated SCFs and MWNTs had synergetic effects on the fracture toughness of the EP. To evaluate the effect of the MWNTs on the internal stress level of the SCF-reinforced composite, the fracture tests were also performed with the relaxed specimens. As shown in Figure 6(b), the K_{IC} values of all of the specimens increased after relaxation. Compared with the SCF-reinforced specimens, this showed an obvious decrease in the internal stress for the multiscale reinforced specimens. This phenomenon was attributed to the redistribution effect of the internal stress realized by the MWNTs during the curing process;[31] this helped us relieve the overstress at the SCF/EP interfaces.

SEM micrographs of the fracture surfaces are shown in Figure 7. Because of the brittleness, the specimen of EP displayed a smooth fracture surface [Figure 7(a)]. After filled with 10-phr untreated SCFs, several holes and concaves were observed on

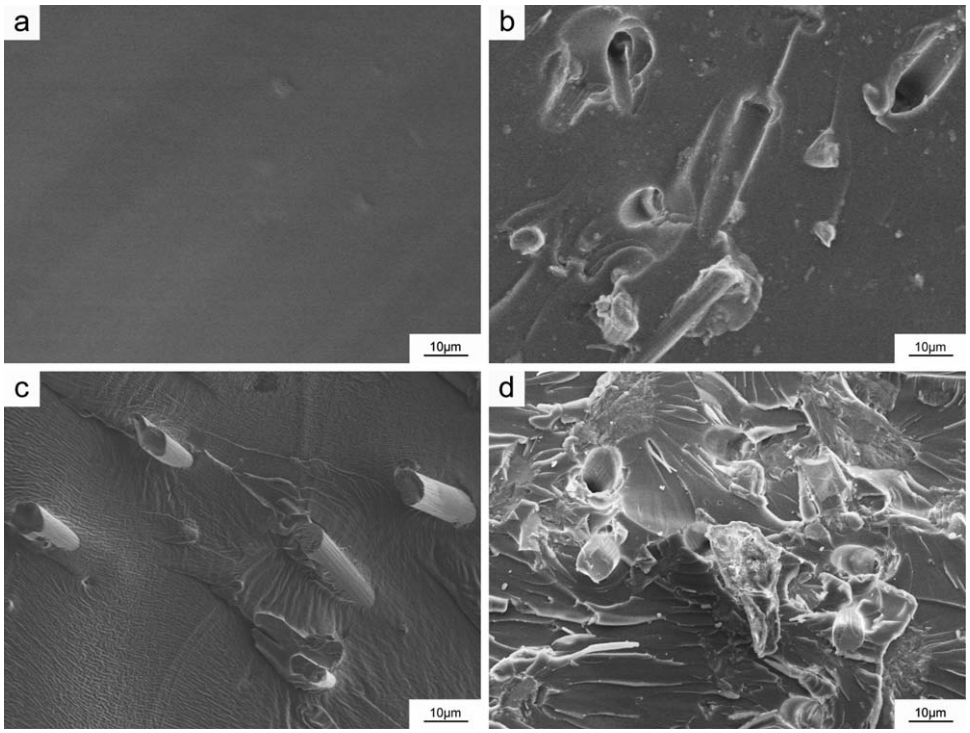

Figure 7. SEM micrographs of the fracture surfaces: (a) EP, (b) 10CF, (c) 10TCF, and (d) 10TCF1NT.

the fracture surface [Figure 7(b)]. On the one hand, these features indicated that the untreated SCFs prevented crack propagation in the matrix by mechanisms of fiber debonding and fiber pullout, so the fracture toughness of 10CF was improved to a certain degree over that of neat EP. On the other hand, they also indicated that the SCF/EP interfaces were not well integrated because the remaining holes and concaves had smooth surfaces. After filling with 10-phr treated SCFs, the integrated conditions of the SCF/EP interfaces were obviously improved [Figure 7(c)]. The increased surface roughness of the SCFs after BMLPO treatment contributed to the interlocking between the SCFs and the matrix. Meanwhile, the improved surface wettability against EP also led to a better interfacial integration. Therefore, when a crack emerged and propagated inside the materials, the treated SCFs prevented it and consumed more energy during their debonding and pullout from the matrix. In comparison with the neat EP and SCF-reinforced specimens, the multiscale composite filled with a combination of treated SCFs and MWNTs (10TCF1NT) showed a rougher fracture surface with more plastic deformation areas [Figure 7(d)]. As shown by the previous results and our previous study, the sole addition of SCFs or MWNTs did not lead to obvious plastic deformation.[42] Therefore, this variation in the fracture morphology implied that the interactions between the treated SCFs and MWNTs may have contributed to the promotion of the plastic deformation of the multiscale composites, such as through shear banding and cavitation growth.

Impact Strength

Figure 8 shows the impact strength results of the notched and unnotched specimens. The neat EP displayed the lowest values of notched and unnotched impact strengths of 2.32 and 12.30 kJ/m^2, respectively. The addition of untreated SCFs increased the notched and unnotched impact strength to 4.15 and 18.5 kJ/m^2; these were increases of 78.9 and 50.4% over than that of the neat EP, respectively. The treated SCFs were more efficient in enhancing the impact strength of the EP, with the corresponding values increasing by 152.2 and 84.1%, respectively. These results indicate that the surface treatment of the SCFs contributed to improvements in the integration conditions of the SCF/EP interface and, thus, increased the capability of restraining the crack propagation inside the composites under dynamic impact loading. Comparatively, the addition of the MWNTs only slightly increased the notched and unnotched

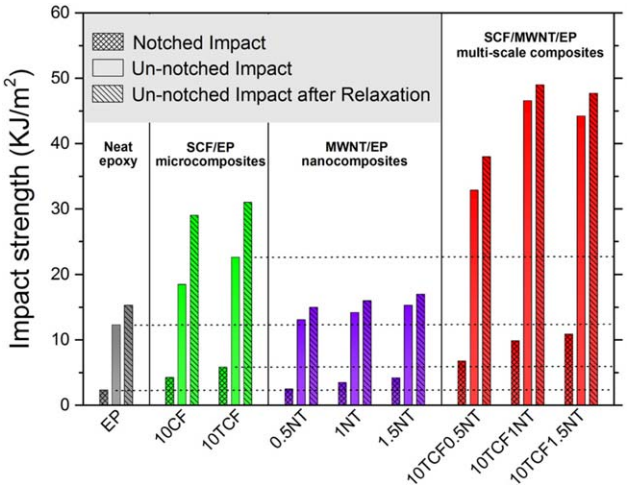

Figure 8. Impact strength of the materials. [Color figure can be viewed in the online issue, which is available at wileyonlinelibrary.com.]

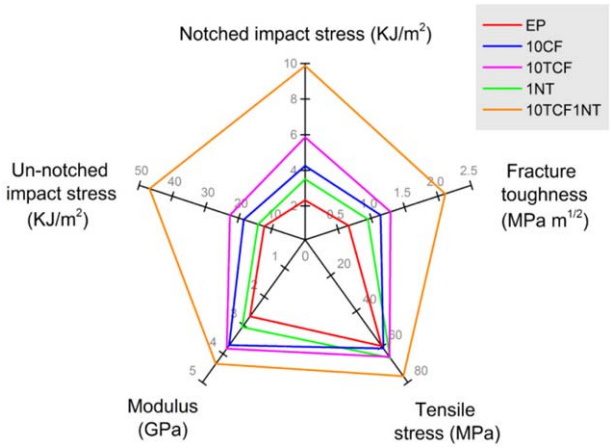

Figure 9. Spider diagram of the absolute values of some typical materials. [Color figure can be viewed in the online issue, which is available at wileyonlinelibrary.com.]

impact strengths. For example, the notched impact strengths of 0.5NT, 1NT, and 1.5NT increased by 7.8, 50.9, and 81.0% over than that of the neat EP, respectively. The unnotched impact strength increased by 6.5, 15.4, and 24.4%, respectively. All of these increase ranges were smaller than that of the SCF-reinforced specimens.

The combined use of the treated SCFs and MWNTs also played synergetic roles in both notched and unnotched impact strengths of the materials. For example, the notched and unnotched impact strengths of 10TCF1NT were 9.86 and 46.58 kJ/m^2, respectively; these were increases of 325.0 and 278.7% over than that of the neat EP. These increases were higher than the total growth of the corresponding binary composites (10TCF and 1NT). The unnotched impact strength after relaxation were also tested to evaluate the effect of the MWNTs on the variation of internal stress level in the cured composites. We found that the addition of the MWNTs also decreased the internal stress level of the multiscale composites. This phenomenon was attributed to the stress-redistribution process and the homogenized stress field caused by the addition of MWNTs; this relieved the overstress at the SCF/EP interfaces during the curing process of the composites.

This showed a significantly higher unnotched impact strength than the single-filler-based composites. For the unnotched specimens, the impact energy consumption was superposed by the initiation of critical cracks and crack propagation. The significant increase in the unnotched impact strength over that of the single-filler-based composites could be explained by the following two aspects. On the one hand, the decreased internal stress caused by the addition of MWNTs generated less microcracks at the SCF/EP interfaces; this helped to reduce the initiation of critical cracks. On the other hand, the relieved overstress at the SCF/EP interfaces contributed to the enhancement of the crack resistance ability of the composites.

To compare the different modification methods on the mechanical performance of the EP more clearly, the main experimental results obtained in this study are illustrated in Figure 9. They show that the brittleness of neat EP with the lowest fracture toughness and impact strength was the shortcoming; this hampers its potential for high-performance applications. The treated SCF-reinforced specimen (10TCF) showed better improvements in the mechanical properties and fracture toughness of the neat EP than the untreated SCF-reinforced ones; this indicated that the surface treatment of the SCFs was necessary and effective. The combination of the treated SCFs and MWNTs significantly improved the tensile strength, elastic modulus, fracture toughness, and impact strength of the neat EP. The addition of multiscale reinforcements made up for the shortcomings of low fracture toughness and impact strength of the neat EP; this will provide a promising way to enhance the overall performance and broaden its applications in engineering areas.

CONCLUSIONS

The BMLPO treatment led to an increase in the surface roughness and a decrease in the contact angle against EP, and thus, the improvement of the interfacial interactions were obtained in the SCF-reinforced composites. The treated SCFs exhibited better reinforcing effects on the tensile strength, elastic modulus, fracture toughness, and impact strength of the neat EP than the untreated ones.

On the basis of Halpin–Tsai equations, a modified model was developed to predict the elastic modulus of the multiscale composites reinforced with a combination of treated SCFs and MWNTs. The results indicate that the relative errors between the experimental and theoretical values were smaller than 10%.

The combined use of the treated SCFs and MWNTs improved the overall mechanical properties of the neat EP. The multiscale reinforcements showed synergetic effects on the tensile strength, fracture toughness, and impact strength. As the DMA results indicated, the addition of MWNTs contributed to the promotion of the interfacial interactions in the multiscale composites. Then, the concentrated stress at the SCF/EP interfaces was redistributed, and the stress field was homogenized by the addition of MWNTs. Moreover, the addition of MWNTs contributed to the promotion of the plastic deformation of the multiscale composites. These aspects are considered the reasons for the synergetic effects.

ACKNOWLEDGMENTS

The authors are grateful to Wei Wang for the use of the AFM equipment and Jie Wang for help with the SEM observations. The authors also express their sincere thanks to Xupu Yang for help with the fracture and impact testing. Thanks are also given to the anonymous reviewers for their helpful suggestions for improving this article.

REFERENCES

1. Khshain, N. T.; Al-Mahaidi, R.; Abdouka, K. *Compos. Struct.* **2015**, *132*, 205.
2. Kanehashi, S.; Yokoyama, K.; Masuda, R.; Kidesaki, T.; Nagai, K.; Msiyakoshi, T. *J. Appl. Polym. Sci.* **2013**, *130*, 2468.

3. Rmili, W.; Deffarges, M. P.; Chalon, F.; Ma, Z.; Leroy, R. *J. Electron. Mater.* **2014**, *43*, 702.
4. Domun, N.; Hadavinia, H.; Zhang, T.; Sainsbury, T.; Liaghat, G. H.; Vahid, S. *Nanoscale* **2015**, *7*, 10294.
5. Garg, A. C.; Mai, Y. W. *Compos. Sci. Technol.* **1988**, *31*, 225.
6. Gulrez, S. K. H.; Mohsin, M. E. A.; Al-Zahrani, S. M. *J. Polym. Res.* **2013**, *20*, 1.
7. Chen, K. U.S. Pat. 7,708,349 (**2010**).
8. Reis, J. M. L.; Ferreira, A. J. M. *Constr. Build. Mater.* **2004**, *18*, 523.
9. Kaynak, C.; Orgun, O.; Tincer, T. *Polym. Test.* **2005**, *24*, 455.
10. Friedrich, K. *Compos. Sci. Technol.* **1985**, *22*, 43.
11. Zhang, G.; Rasheva, Z.; Karger-Kocsis, J.; Burkhart, T. *Express Polym. Lett.* **2011**, *5*, 859.
12. Ajayan, P. M. *Chem. Rev.* **1999**, *99*, 1787.
13. Micusik, M.; Omastova, M.; Krupa, I.; Prokes, J.; Pissis, P.; Logakis, E.; Pandis, C.; Potschke, P.; Pionteck, J. *J. Appl. Polym. Sci.* **2009**, *113*, 2536.
14. Khurram, A. A.; Rakha, S. A.; Ali, N.; Zhou, P. H.; Munir, A. *J. Appl. Polym. Sci.* **2014**, *131*, 1366.
15. Hueso, L. E.; Pruneda, J. M.; Ferrari, V.; Burnell, G.; Valdes-Herrera, J. P.; Simons, B. D.; Littlewood, P. B.; Artacho, E.; Fert, A.; Mathur, N. D. *Nature* **2007**, *445*, 410.
16. Martone, A.; Formicola, C.; Giordano, M.; Zarrelli, M. *Compos. Sci. Technol.* **2010**, *70*, 1154.
17. Song, K. A.; Zhang, Y. Y.; Meng, J. S.; Green, E. C.; Tajaddod, N.; Li, H.; Minus, M. L. *Materials* **2013**, *6*, 2543.
18. Potts, J. R.; Dreyer, D. R.; Bielawski, C. W.; Ruoff, R. S. *Polymer* **2011**, *52*, 5.
19. Montazeri, A.; Javadpour, J.; Khavandi, A.; Tcharkhtchi, A.; Mohajeri, A. *Mater. Des.* **2010**, *31*, 4202.
20. Godara, A.; Mezzo, L.; Luizi, F.; Warrier, A.; Lomov, S. V.; van Vuure, A. W.; Gorbatikh, L.; Moldenaers, P.; Verpoest, I. *Carbon* **2009**, *47*, 2914.
21. Gkikas, G.; Barkoula, N. M.; Paipetis, A. S. *Compos. B* **2012**, *43*, 2697.
22. Ritchie, R. O. *Nat. Mater.* **2011**, *10*, 817.
23. Rahmanian, S.; Suraya, A. R.; Shazed, M. A.; Zahari, R.; Zainudin, E. S. *Mater. Des.* **2014**, *60*, 34.
24. Zhang, G.; Karger-Kocsis, J.; Zou, J. *Carbon* **2010**, *48*, 4289.
25. Sharma, S. P.; Lakkad, S. C. *Surf. Coat. Technol.* **2010**, *205*, 350.
26. Chen, Q.; Zhang, L.; Zhao, Y.; Wu, X. F.; Fong, H. *Compos. B* **2012**, *43*, 309.
27. Kinloch, A. J.; Lee, J. H.; Taylor, A. C.; Sprenger, S.; Eger, C.; Egan, D. *J. Adhes.* **2003**, *79*, 867.
28. ASTM D 5045-99, Standard Test Methods for Plane-Strain Fracture Toughness and Strain Energy Release Rate of Plastic Materials; ASTM International: West Conshohocken, PA, **1999**.
29. Kinloch, A. J. Adhesion and Adhesives: Science and Technology; Chapman & Hall: London, **1987**.
30. Rashkovan, I. A.; Korabelnikov, Y. G. *Compos. Sci. Technol.* **1997**, *57*, 1017.
31. Chen, Z. K.; Yang, G.; Yang, J. P.; Fu, S. Y.; Ye, L.; Huang, Y. G. *Polymer* **2009**, *50*, 1316.
32. Tzeng, S. H.; Tsai, J. L. *J. Reinf. Plast. Compos.* **2011**, *30*, 922.
33. Hameed, A.; Islam, M.; Ahmad, I.; Mahmood, N.; Saeed, S.; Javed, H. *Polym. Compos.* **2015**, *36*, 1891.
34. Jyotishkumar, P.; Logakis, E.; George, S. M.; Pionteck, J.; Haussler, L.; Hassler, R.; Pissis, P.; Thomas, S. *J. Appl. Polym. Sci.* **2013**, *127*, 3063.
35. Affdl, J. C.; Kardos, J. L. *Polym. Eng. Sci.* **1976**, *16*, 344.
36. Balakrishnan, A.; Saha, M. C. *Mater. Sci. Eng. A* **2011**, *528*, 906.
37. Lu, J. P. *J. Phys. Chem. Solids* **1997**, *58*, 1649.
38. Cui, H.; Kessler, M. R. *Compos. Sci. Technol.* **2012**, *72*, 1264.
39. Abdalla, M.; Dean, D.; Robinson, P.; Nyairo, E. *Polymer* **2008**, *49*, 3310.
40. Keusch, S.; Haessler, R. *Compos. A* **1999**, *30*, 997.
41. Iisaka, K.; Shibayama, K. *J. Appl. Polym. Sci.* **1977**, *22*, 3135.
42. Zhang, Z.; Tan, Y.; Wang, X.; Tan, H.; Li, J. *Polym. Compos.* **2015**, *36*, 2147.